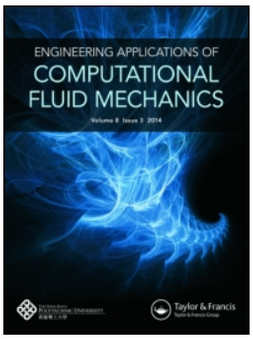

Engineering Applications of Computational Fluid Mechanics

ISSN: 1994-2060 (Print) 1997-003X (Online) Journal homepage: https://www.tandfonline.com/loi/tcfm20

Experimental and computational fluid dynamics-based numerical simulation of using natural gas in a dual-fueled diesel engine

Eivaz Akbarian, Bahman Najafi, Mohsen Jafari, Sina Faizollahzadeh Ardabili, Shahaboddin Shamshirband & Kwok-wing Chau

To cite this article: Eivaz Akbarian, Bahman Najafi, Mohsen Jafari, Sina Faizollahzadeh Ardabili, Shahaboddin Shamshirband & Kwok-wing Chau (2018) Experimental and computational fluid dynamics-based numerical simulation of using natural gas in a dual-fueled diesel engine, Engineering Applications of Computational Fluid Mechanics, 12:1, 517-534, DOI: 10.1080/19942060.2018.1472670

To link to this article: https://doi.org/10.1080/19942060.2018.1472670

Published online: 18 Jun 2018.

ENGINEERING APPLICATIONS OF COMPUTATIONAL FLUID MECHANICS
2018, VOL. 12, NO. 1, 517–534
https://doi.org/10.1080/19942060.2018.1472670

Taylor & Francis
Taylor & Francis Group

Experimental and computational fluid dynamics-based numerical simulation of using natural gas in a dual-fueled diesel engine

Eivaz Akbarian[a], Bahman Najafi[a], Mohsen Jafari[b], Sina Faizollahzadeh Ardabili[a], Shahaboddin Shamshirband[c,d] and Kwok-wing Chau[e]

[a]Biosystem Engineering Department, University of Mohaghegh Ardabili, Ardabil, Iran; [b]Motorsazan Co., Tabriz, Iran; [c]Department for Management of Science and Technology Development, Ton Duc Thang University, Ho Chi Minh City, Vietnam; [d]Faculty of Information Technology, Ton Duc Thang University, Ho Chi Minh City, Vietnam; [e]Department of Civil and Environmental Engineering, Hong Kong Polytechnic University, Hong Kong, People's Republic of China

ABSTRACT

In this paper, investigations were performed on a dual-fueled constant-speed engine. Initially, the emissions and performance of a diesel engine were investigated, and after moving to the dual-fuel engine, experimental tests were carried out under different loads (10, 25, 50, 75, and 100% of the full load) and pilot to gaseous fuel (PGF) ratios (30, 40, and 50%). The results showed that under different loads and PGF ratios, the emissions of nitrous oxides and particle materials in the dual mode were lower than those for the diesel engine, and that the difference was significant. The emission of carbon dioxide in the dual-fueled mode varied little compared to that of the diesel mode, although it was lower than that for the diesel engine. In loads lower than 75% of the full load, the emission of carbon monoxide in the diesel engine was lower than that for the dual-fueled engine. However, in full load, this result was reversed and had significant difference. The dual mode had lower hydrocarbon emission compared to that of the diesel mode in all PGF ratios and loads. A computational fluid dynamics-based numerical simulation was performed by KIVA3V, and its results showed good agreements with the experimental results under cylinder pressure.

ARTICLE HISTORY
Received 22 January 2018
Accepted 1 May 2018

KEYWORDS
computational fluid dynamics; dual-fueled diesel engine; engine performance; emissions; natural gas

Nomenclature

$(AFR_{NG})_{Stoic}$	Stoichiometric air fuel ratios for NG
$(AFR_{PF})_{Stoic}$	Stoichiometric air fuel ratios for diesel fuel
DF 30%	Dual-fuel mode with pilot fuel to gaseous fuel: 30%
DF 40%	Dual-fuel mode with pilot fuel to gaseous fuel: 40%
DF 50%	Dual-fuel mode with pilot fuel to gaseous fuel: 50%
E_A	Activation energy
$\dot{H}_{pilotfuel}$	Heating energy rates of the pilot fuel
$\dot{H}_{NG}$	Heating energy rates of the NG
$LHV_{pilotfuel}$	Lower heating values of the pilot fuel (MJ/kg)
LHV_{NG}	Lower heating values of the NG (MJ/m^3)
M_{PS}	Mean piston speed (m/s)
$\dot{m}_g$	Mass flow rate of the pilot fuel (g/h)
$\dot{m}_{PF}$	Mass flow rate of pilot fuel (g/h)
$\dot{m}_{NG}$	Natural gas mass flow rate in dual-fuel operating mode (g/h)
$\dot{m}_{air}$	Mass flow rates of air (g/h)
N	Engine speed (rpm)
n	Polytropic index of compression
O_{df}	Oxygen concentration of the dual- fuel engine
O_f	Oxygen mole fraction
t	time
u	Fluid velocity
V	In-cylinder volume
γ	Ratio of specific heats
ρ_m	Mass density of species m
ρ	Total mass density
τ_i	Ignition delay (crank angle)

Introduction

The supply of energy by using different low-cost resources with lower carbon footprints is an on-going research interest. This has been further motivated by the fact that fossil fuels as energy carriers are depleting and, more importantly, that their large-scale utilization

CONTACT Bahman Najafi najafib@uma.ac.ir

is a major cause of environmental pollution. The atmospheric concentration of carbon dioxide CO_2 stands at 400 parts per million (ppm) and is anticipated to grow by 2 ppm every year (Murty, 1975). The emissions from diesel engines, especially particle materials (PM), pose serious harm to both the environment and human health (Arteconi, Brandoni, Evangelista, & Polonara, 2010). Diesel fuel is derived from non-renewable petroleum oil and will be completely consumed within a few decades. With increasing concerns over pollution from the burning of fossil fuels and energy security, the development and application of alternative fuels has become a crucial subject at present (Mintz, Han, & Burnham, 2014). Methane is a simple hydrocarbon with high hydrogen to carbon ratio without any C–C bonding, thereby causing clean combustion compared to other fossil fuels (Sahoo, Sahoo, & Saha, 2009). Therefore, using methane with diesel fuel in a dual combustion is a potential route to reduce pollution in urban and industrial zones (Di Iorio, Magno, Mancaruso, & Vaglieco, 2017). Natural gas (NG) is a hydrocarbon gas mixture primarily consisting of methane (Mittal, Donahue, Winnie, & Gillette, 2015).

Dual fueling with diesel–NG is one of the approaches among the various strategies considered for achieving cleaner combustion in the internal combustion engines (Abagnale et al., 2014b). Diesel–NG dual-fueled operation is generally characterized by using diesel as a pilot injection to start the combustion in a chamber with NG/air mixture (Abagnale et al., 2014a). Dual-fueled combustion is one of the easy and low-cost approaches to replace with conventional diesel engines to reduce fuel cost and exhaust emissions (Maghbouli, Saray, Shafee, & Ghafouri, 2013).

Diesel–NG combustion provides a suitable condition to reduce PM and nitrogen oxides (NO_x) emissions compared to diesel ignition engines (Barik & Murugan, 2014; Mustafi, Raine, & Verhelst, 2013). CO_2 pollutant levels can be reduced in the dual-fueled combustion mode (Lounici et al., 2014), although carbon monoxide CO and unburnt hydrocarbon (UHC) emissions increase in the dual-fuel engine (Di Iorio, Magno, Mancaruso, & Vaglieco, 2016). The use of exhaust gas recirculation (EGR) (Lipardi, Versailles, Watson, Bourque, & Bergthorson, 2017; Papagiannakis, 2013; Singh Kalsi & Subramanian, 2016; Zhao, Wang, Li, Lei, & Liu, 2014), throttle control (Ling, Longbao, Shenghua, & Hui, 2005), modified combustion chamber geometry (Lee & Park, 2017), intake valve timing (Jung, Song, & Hur, 2017), advancing the pilot fuel injection time (Wang et al., 2016; Yang, Xi, Wei, Zeng, & Lai, 2015) and the use of biofuels (Jamuwa, Sharma, & Soni, 2016; Najafi, 2011; Najafi, Piirouzpanah, Ghobadian, Sadegpour, & Ranjbar, 2007; Najafi, Torkian, Hejazi, & Zamzamian, 2011; Yoon & Lee, 2011) have been suggested to overcome high emissions of CO and UHC from dual-fuel engines. Such operations and their different aspects have been employed to improve the engine emissions and performance.

For instance, Yaliwal et al. (2016) studied the relation of engine performance and combustion chamber geometry in a dual-fueled diesel engine fueled by Honge methyl ester and producer gas. They used three types of fuel injectors with 3, 4, and 5 holes as well as varying pressures from 210 up to 240 bar and two types of combustion chamber to find proper matches of injectors and combustion chamber for the highest engine performance. Zhang and Song (2016) studied the combustion process in order to utilize liquid natural gas (LNG) on an electronically controlled common rail dual (diesel–NG) engine. In their study, the brake specific fuel consumption (BSFC) and the exhaust emissions under varied co-combustion ratios and speeds of 1200 rpm and 2200 rpm were compared and analyzed. Mikulski and Wierzbicki (2016) studied the relation of gas composition and combustion characteristics of a four-cylinder, dual-fuel (diesel–NG), turbocharged, direct injection engine. Based on results, ignition delay (ID) of the initial diesel dose has been significantly affected by the changes of the gas composition.

Lounici, Boussadi, Loubar, and Tazerout (2014) studied the effect of enriched NG with various H_2 blends on dual-fueled engine. Based on experimental results, total hydrocarbons (THC), CO_2, and CO emissions have been reduced by using gaseous fuel, but NO_x emission increased slightly. Pan, Yao, Han, Wei, and Wang (2015) studied the effect of intake air temperature (IAT) on the emissions and performance of a dual (diesel/methanol) fueled engine. Based on results, decreasing the IAT prolonged ID and reduced the peak cylinder pressure; while increasing the IAT reduced the emissions of CO, THC, NO_2, methanol and formaldehyde and increased soot, NO_x and NO emissions. In a different study, Lata and Misra (2010) developed mathematical models to estimate pressure, mean gas temperature, net heat release rate (HRR), and brake thermal efficiency in the case of using a dual (hydrogen/liquid petroleum gas (LPG)) fueled engine. The output of the proposed model had a high correlation with the experimental results.

Kumar and Raj (2013) studied the effects of fuel injection timing (FIT) and IAT on the emission and performance of an air-cooled, single-cylinder, four-stroke, dual (biodiesel/ethanol) fueled engine. Based on the results, increasing the injection timing increases exhaust temperature, in cylinder pressure, HRR, and NO_x emission, and decreases CO and HC emissions. (Ge, Kim, Yoon, & Choi, 2015; Yoon, Kim, Kim, & Choi, 2014).

Combustion in dual-fueled engines is more complex because it has both diesel-cycle and Otto-cycle dual characteristics. Increasing the co-combustion ratio decreases the diffusive combustion of pilot diesel fuel. The emissions generation mechanism of dual-fueled systems falls between those of diesel diffusion combustion and NG flame propagation combustion (Zhang & Song, 2016).

Therefore, it is important to study the effect of fuel combinations on the performance and emissions of a dual-fueled engine. In general, the dual-fueled engine's performance is lower than the same diesel engine (Papagiannakis & Hountalas, 2003, 2004; Yoon & Lee, 2011), but one of the purposes of this work was to achieve the level of diesel engine performance in a dual-fueled mode.

The present work was set to experimentally and theoretically investigate the performance and emission characteristics of a dual (NG/diesel (as pilot fuel)) fueled engine at 10, 25, 50, 75, and 100% of full load. The pilot FIT, and pilot to gaseous fuel (PGF) ratios were the two main factors of study. In fact, the aim of this work was to convert a conventional diesel engine to a dual-fueled engine in order to decrease emissions while maintaining engine performance (engine brake power). Computational fluid dynamics (CFD) was also carried out to understand the combustion phenomena in the dual-fuel mode.

Experimental setup and procedure

Engine and test facilities

The engine under investigation was a direct injection, four-cylinder diesel engine with a constant-speed (1500 rpm) that is typically used in generators and water pumps. The characteristics of the engine have been tabulated in Table 1. The engine was equipped with an electronically governed distributor injection pump and a four-hole injector to reach an injection pressure of 270 bar. All the experimental tests were performed in the MOTORSAZN R&D department test cell. The instrument specifications used for the experimental tests are shown in Table 2. The engine speed had been kept at 1500 rpm under all test conditions. After connecting the engine to a dynamometer (eddy current absorption dynamometer, SCHENK W700), tests were performed on the diesel engine with different loads including 10, 25, 50, 75, and 100% of the full load based on the ECE-R96 standard for steady-state constant speed engines (Table 3), and then the exhaust emissions were measured (AVL DICOM 4000) under each test condition. Engine

Table 1. Engine characteristics.

Characteristic	Value
No. of cylinder	4, Inline
Cycle	Four strokes
Aspiration	Natural
Engine volume (lit)	4
Bore (mm)	100
Stroke (mm)	127
Compression ratio	16:1
Injection	Direct
Rating	44 kW@1500 rpm

Table 2. Measurement instruments specifications.

Measurement	Instrument	Range	Resolution
NO_x	AVL DICOM 4000 (Non-Dispersive Infra-Red Technique)	0–4000 ppm	1 ppm
HC		0–200,000 ppm by vol.	1 ppm
CO		0–10% by vol.	0.001%Vol.
CO_2		0–20% by vol.	0.01% Vol.
λ		0–10	0.001
PM	AVL 415S	0–10	0.001
In-cylinder pressure	AVL GU 13G & AVL Micro IFEM Piezo		0.001 bar @ 0.1° CA
Data acquisition system	LabVIEW-based & IndiCom		
Air flow rate	ABB Sensyflow P	0–400 m^3/h	±0.1 m^3/h
Diesel flow rate	Rizpoya		0.001 kg/h
NG flow rate	GAS SUZAN (AG 75.10)		0.001 m3
Temperatures	Grant Eltek 1000 Series & K type termocouple	−50–1600°C	0.1°C
Injection time	AVL SL31D 2000 & AVL Dicom 4000		0.1° CA
Engine torque	SCHENK Dynamometer	0–700 kW	0.1 N.m
Engine speed	SCHENK	0–10000 rpm	1 rpm
Crank angle	AVL 365C		0.1 CA

Table 3. ECE-R96 standard for testing constant speed engine.

Mode	Torque (%)	Engine Speed	Engine Speed
1	100	Rated	Rated
2	75	Rated	Rated
3	50	Rated	Rated
4	25	Rated	Rated
5	10	Rated	Rated

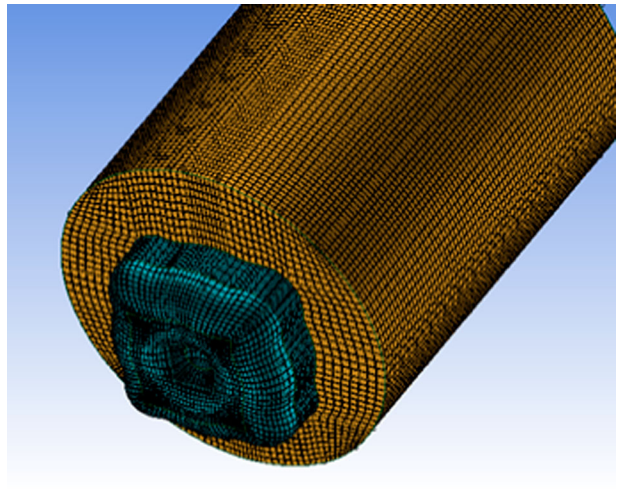

Figure 1. Meshing combustion chamber.

torque and fuel consumption were recorded by a data acquisition system (LabVIEW-based & IndiCom) and a dynamometer. The diesel FIT was measured by an AVL 365C crank angle encoder. A piezoelectric pressure transducer (IFEM Piezo) with quartz crystals was used to measure the engine's in-cylinder pressure.

Table 4. Kinetics reactions used in simulations (Turns, 2000).

1	$2DF2 + 37O_2 \rightarrow 24CO_2 + 26H_2O$
2	$O_2 + 2N_2 \rightarrow 2N + 2NO$
3	$2O_2 + N_2 \rightarrow 2O + 2NO$
4	$N_2 + 2OH \rightarrow 2H + 2NO$
5	$2O_2 + CH_4 \rightarrow CO_2 + 2H_2O$
6	$O + CO_2 \rightarrow O_2 + CO$
7	$O_2 + N \rightarrow O + NO$
8	$OH + CO \rightarrow H + CO_2$
9	$N_2 + O \rightarrow N + NO$
10	$O_2 + H \rightarrow OH + O$

Table 5. Equilibrium reactions used in simulations (Turns, 2000).

1	$H_2 \rightleftharpoons 2H$
2	$O_2 \rightleftharpoons 2O$
3	$N_2 \rightleftharpoons 2N$
4	$O_2 + H_2 \rightleftharpoons 2OH$
5	$O_2 + 2H_2O \rightleftharpoons 4OH$
6	$O_2 + 2CO \rightleftharpoons 2CO_2$

Engine performance simulation

Numerical investigations were performed by adopting KIVA 3V code to estimate in-cylinder pressure and temperature under different conditions of loads and pilot injection timing and quantities. First, the combustion chamber was modeled in Solid Works® software (Dassault system Co. Ver 2015) using piston geometry and the engine manufacturer's data. Then the combustion chamber meshing was developed by ANSYS-ICEM® (Ansys software Co. Ver R16). Figure 1 shows the combustion chamber after meshing. To prove the mesh's independency of the calculations, mesh generating was performed by 12964, 16619, and 22175 elements. Reducing the mesh size after achieving a reasonable convergence in results is worthless, and it only leads to increase in the time for calculations. The simulation results showed that 16619 and 22175 elements had little difference in cylinder pressure simulations, and then calculations were carried out with 16619 elements to save time.

The ICEM outputs and other engine data were imported to the KIVA 3V code. The KIVA 3V code was modified by some settings and extra subroutines to estimate cylinder pressure, temperature and ID. The methane content in NG composition was higher than 96

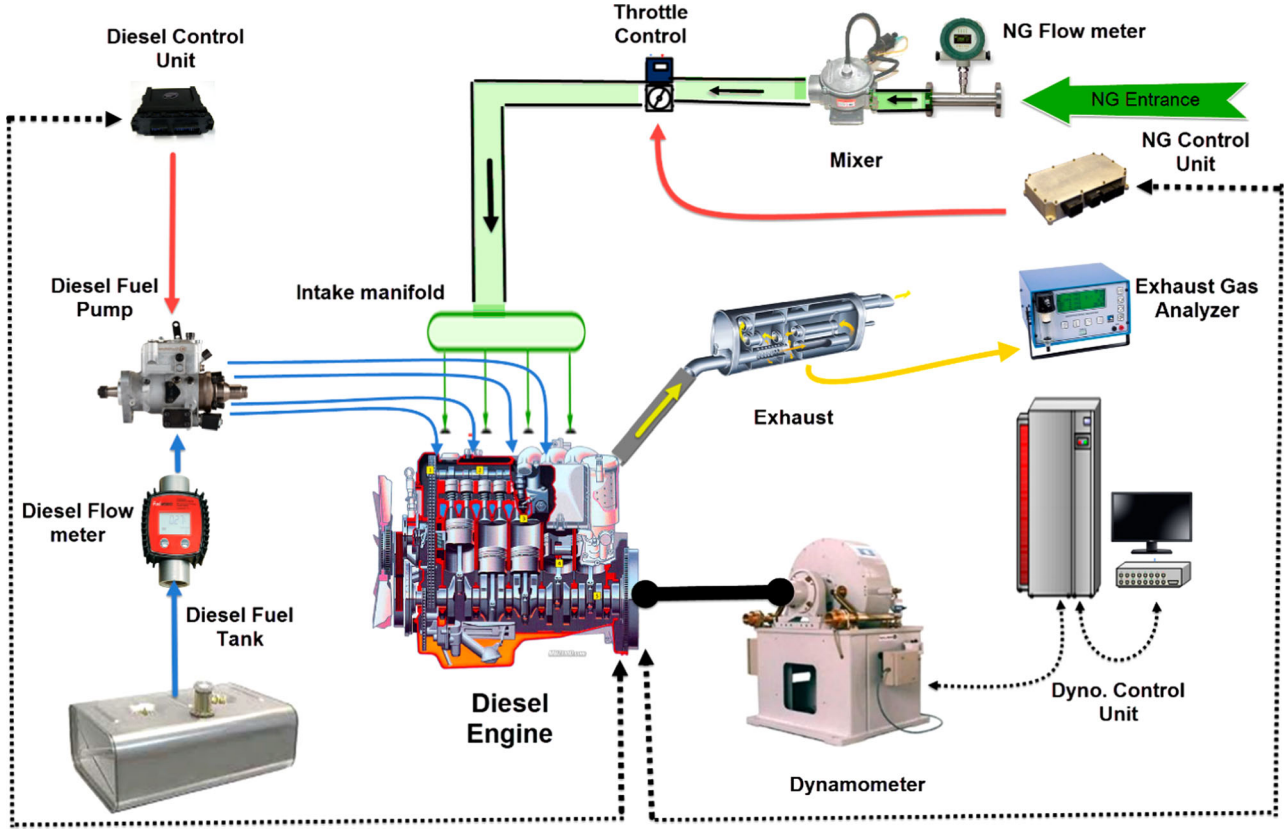

Figure 2. The dual-fueled engine schematic.

Vol. % and, for the purpose of simulation, was assumed to be 100 Vol. %. In this work, 13 species (N_2, O_2, H_2O, CO_2, H_2, H, OH, O, N, CO, NO, diesel fuel, and CH_4 (gaseous fuel)), 10 kinetic reactions and six equilibrium equations were employed in the KIVA code as shown in Tables 4 and 5. A $k-\varepsilon$ turbulent model was used for the CFD simulations with the KIVA code. Equations (1), (2) and (3) present, respectively, the continuity equation for a species and fluid momentum and energy equations in terms of specific internal energy (Rosen, 1989):

$$\frac{\partial \rho_{\mathrm{m}}}{\partial t}+\nabla\cdot(\rho_{\mathrm{m}}\mathbf{u})=\nabla.\left[\rho D\nabla\left(\frac{\rho_{\mathrm{m}}}{\rho}\right)\right]+\dot{\rho}^{c}_{\mathrm{m}}+\dot{\rho}^{s}\delta_{m1} \tag{1}$$

$$\frac{\partial(\rho\mathbf{u})}{\partial t}+\nabla.(\rho_{\mathrm{m}}\mathbf{uu})=-\frac{1}{a^2}\nabla p-A_0\nabla\left(\frac{2}{3}\rho k\right)+\nabla.\boldsymbol{\sigma}+F^{s}+\rho g \tag{2}$$

$$\frac{\partial(\rho \mathrm{I})}{\partial t}+\nabla\cdot(\rho\mathbf{u}\mathrm{I})=-\rho\nabla\cdot\mathbf{u}+(1-\mathrm{A}_0)\sigma/\nabla\mathbf{u}-\nabla\cdot\mathbf{J}+A_0\rho\varepsilon+\dot{Q}^{c}+\dot{Q}^{s} \tag{3}$$

Table 6. Fuels characteristics (Iranian Research Institute of Petroleum Industry).

Characteristic	NG	Diesel Fuel
Auto ignition (°C)	650	316
Octane number	130	–
Cetane number	–	55
Calorific value (MJ/kg)	48.6	42.1
Carbon content (%)	75	87
Stoichiometric ratio	17.2	14.69

The equations for D and source term due to $\dot{\rho}^{c}_{m}$, $\dot{\rho}^{s}$, $\dot{Q}^{c}$ and $\dot{Q}^{s}$ are illustrated in reference (Rosen, 1989).

Engine cylinder pressure and temperature simulations were performed in the diesel mode primarily, and then gaseous fuel (CH_4) was added to the reactions for simulation of the dual-fuel mode. The apparent net HRR, denoted by (dQ_n/dt), was calculated using Equation (4) (Pedrozo, May, Dalla Nora, Cairns, & Zhao, 2016):

$$\frac{dQ_n}{dt}=\frac{\gamma}{\gamma-1}p\frac{dV}{dt}+\frac{\gamma}{\gamma-1}V\frac{dp}{dt} \tag{4}$$

The engine valve timings, diesel fuel injection profile and its pressure and other necessary data were obtained from the manufacturer's documents.

ID time is an important factor in internal combustion engines. A subroutine code was added to the KIVA code to estimate the ID time in the dual-fueled mode by using Equation (5) (Prakash, Shaik, & Ramesh, 1999):

$$\tau_{i(\mathrm{CA})}=C(O_{df})^{k}(0.36+0.22M_{\mathrm{PS}})\exp\left[E_{\mathrm{A}}\left(\frac{1}{RT_m(r_c)^{n-1}}-\frac{1}{17190}\right)+\left(\frac{21.2}{P_m(r_c)^{n}-12.4}\right)^{0.63}\right] \tag{5}$$

Activation energy E_{A} is given by Equation (6):

$$E_{\mathrm{A}}=\frac{618840}{\mathrm{CN}+25} \tag{6}$$

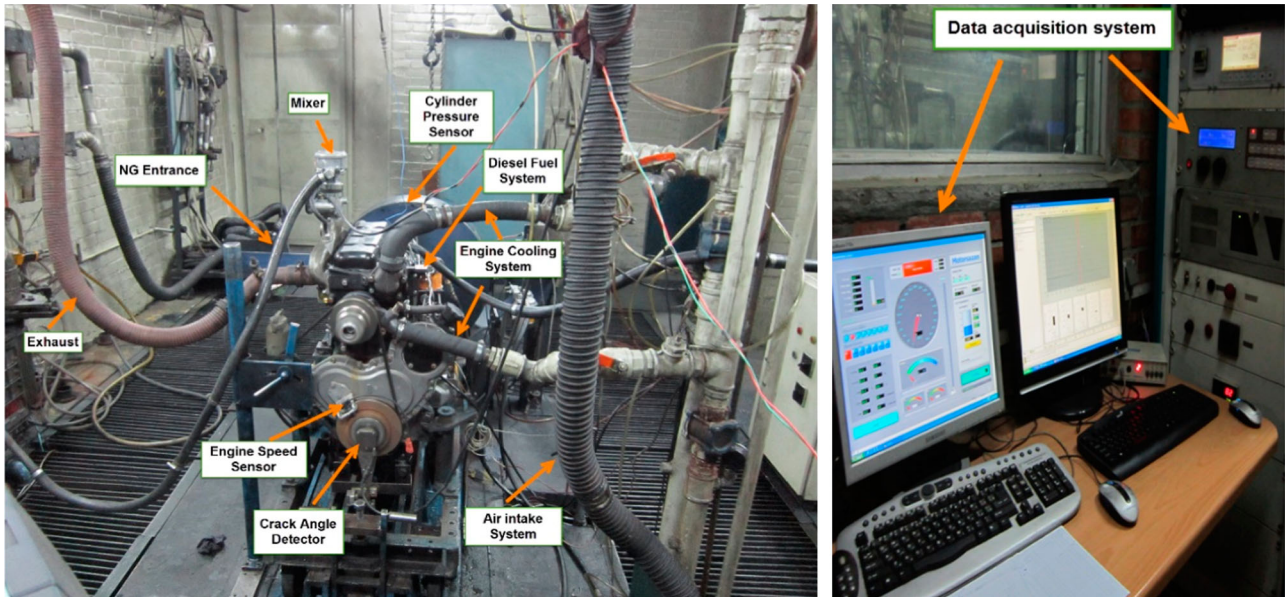

Figure 3. Dual-fueled engine testing in test cell.

where O_{df} is defined as follows:

$$O_{df} = \frac{(O_f)_{\text{dualfuel}}}{(O_f)_{\text{diesel}}} \tag{7}$$

Procedures

The engine can operate in normal diesel- and dual-fueled modes. After finishing the experimental tests in the diesel mode, the engine was converted to the dual-mode (diesel–NG) by a gas mixer, NG control unit, throttle control device, and a suitable hose and connections. Natural gas was mixed with air by a mixer, and then the homogeneous NG–air mixture was passed into the combustion chamber by way of the engine intake manifold. The homogeneous charge was ignited by a pilot diesel injection. There are many ignition points from where combustion starts, and then the flame propagates spontaneously and by pilot fuel flame interaction. NG flow was measured by a gas flow meter (Gas Suzan AG 75.10). The air-gas mixture was passed into the intake manifold and was restricted by a throttle control unit. Figure 2 illustrates a schematic diagram of the dual-fuel engine configuration.

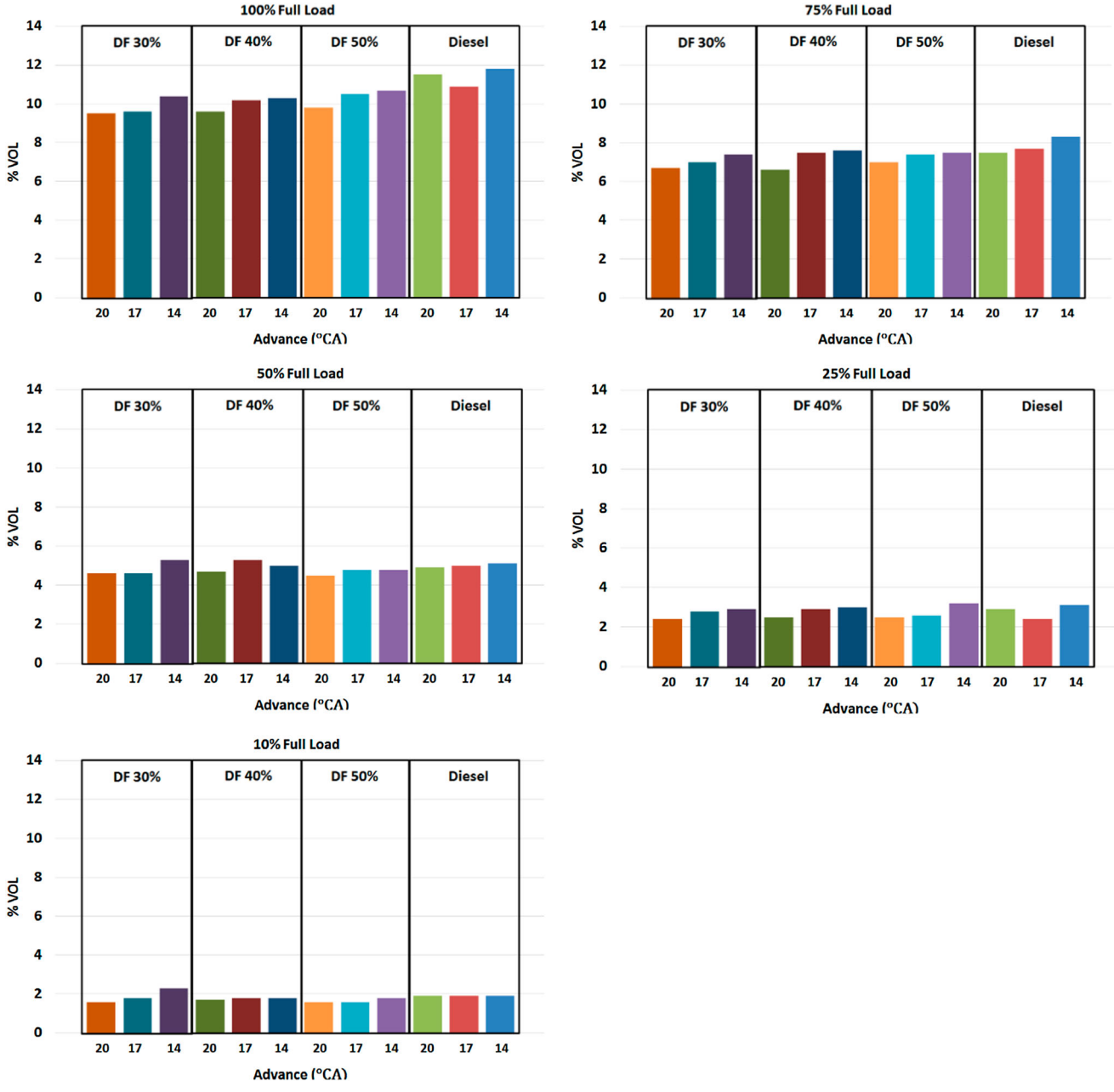

Figure 4. CO_2 emission based on injection timings.

The dual mode pilot fuel (diesel fuel) to NG ratios were 30, 40 and 50%, and the pilot injection timings were 14, 17, 20 degrees of the crank angle (CA) before top dead center (TDC). The PGF ratio was obtained by Equation (8) (Tarabet et al., 2014):

$$Z(\%) = 100 \times \frac{\dot{m}_g}{\dot{m}_g + \dot{m}_{PF}} \tag{8}$$

The quantity of pilot fuel (diesel) injection was adjusted by a fuel control level on the fuel injection pump to 30, 40, and 50% of diesel mode, and then the engine power was raised up to the diesel mode by flowing the NG–air mixture into the intake manifold. The primary application for the original engine type is water pumping or electricity generating, meaning that steady and reliable working of the engine is required. Ratios lower than 30% for PGF (especially at low loads) caused dangerous vibrations of the engine. Therefore, the investigations were continued with 30, 40 and 50% ratios. The diesel fuel and NG characteristics are presented in Table 6.

Natural gas content in intake air was increased until the dual-fuel engine brake power rose to the diesel mode, and then the gaseous fuel consumption

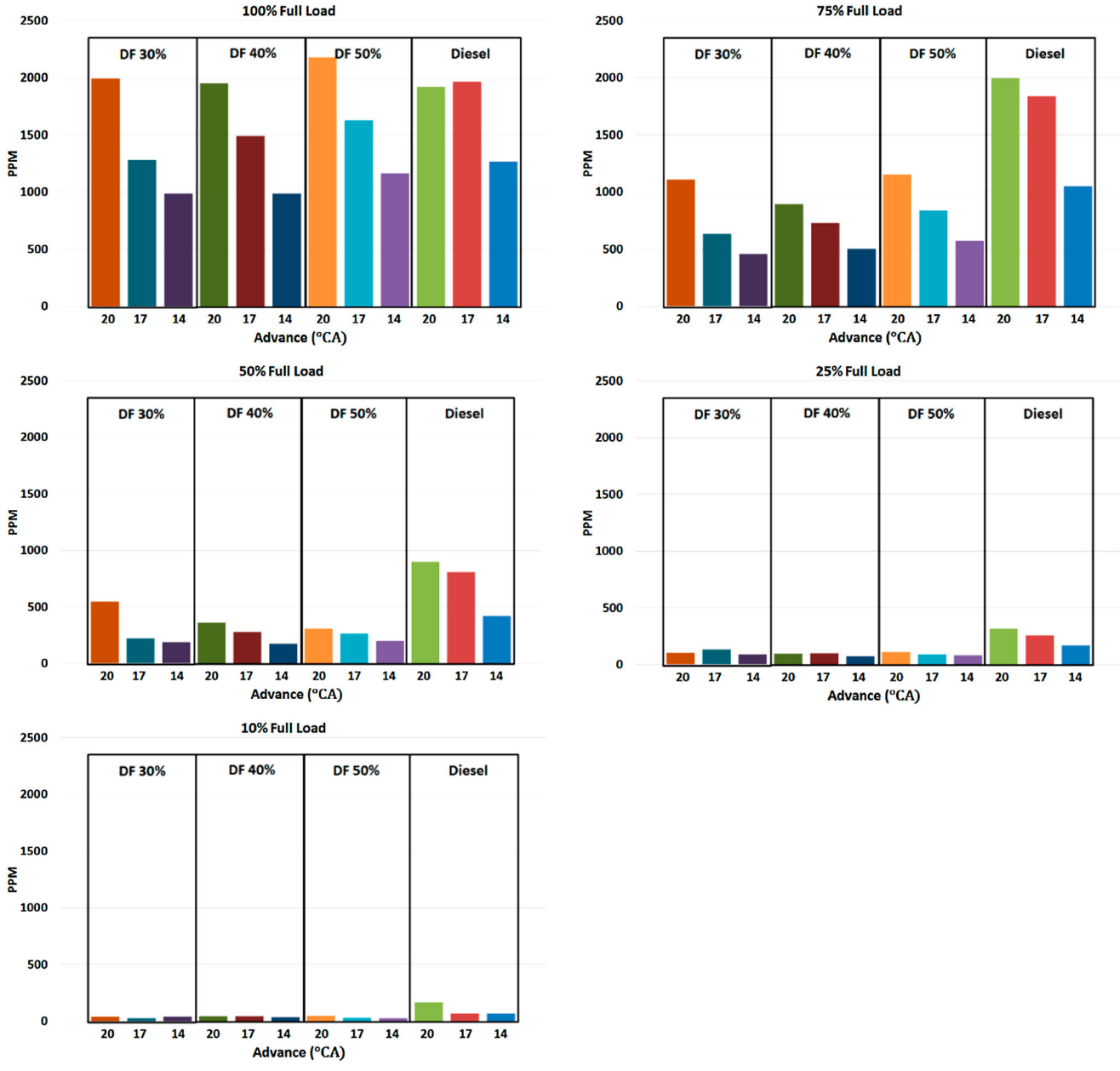

Figure 5. NO_x emission for different pilot injection timings and quantities.

and the engine emissions were recorded by a gas flow meter and an engine pollutant detector (AVL DCOM 4000), respectively. Figure 3 presents the engine test cell.

The engine emissions, its performance and fuel (pilot and gaseous) consumptions were recorded under different loads, pilot injection timings and quantities.

Results and discussions

Figure 4 shows that for the majority of the loads and PGF ratios and different pilot FIT, the emission of CO_2 in dual mode is lower than that of the diesel mode. CO_2 is a complete combustion product. As shown in Figure 4 with increasing load, the amount of CO_2 is also increased. Decreasing PFG ratio (increasing the gaseous fuel portion) reduces CO_2 emission. This indicates that reducing the pilot fuel portion reduces the flame propagation and leads to incomplete combustion. Increasing the gaseous fuel portion and also increasing the FIT decrease the CO_2. The formation of CO_2 correlates with other emissions such as UHC and CO and the amount of CO_2 affected their quantities.

NO_x emission in dual mode is lower than that of the diesel mode for all engine loads, pilot fuel portions

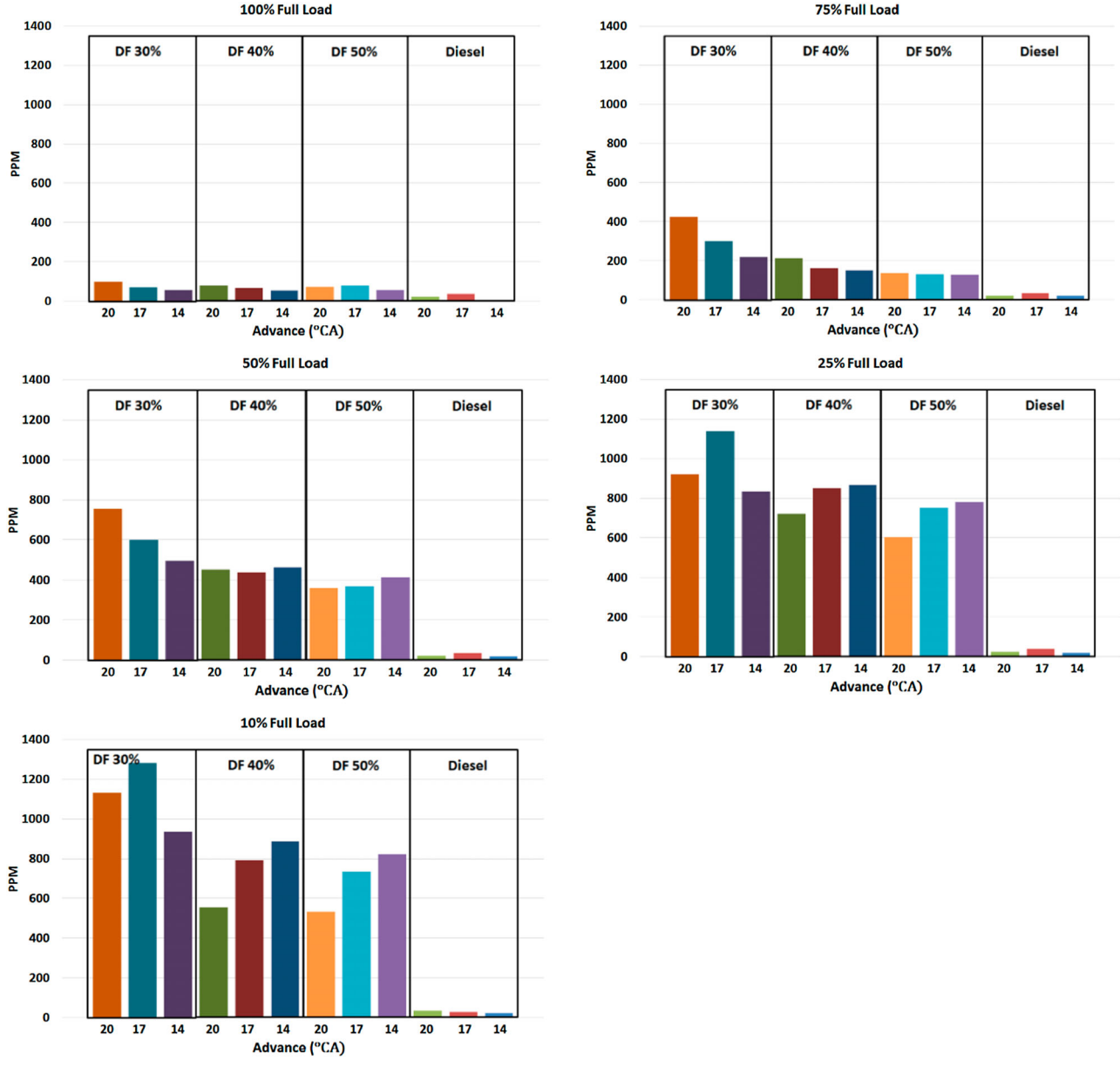

Figure 6. UHC emission for different pilot injection timings and quantities.

and injection timings (Figure 5). Also, decreasing the portion of pilot fuel decreases the NO_x emission. Increasing the pilot injection timing increases NO_x emission for all loads and pilot injection quantities. It might be expected that pilot injection quantity has little effect on NO_x emission, but increasing it increases NO_x formation. We note that NO_x formation depends on the local temperature inside the combustion chamber. In the dual mode, the flame is accompanied by pilot fuel propagation, therefore decreasing diesel fuel (pilot fuel) in the dual mode decreases the local temperature in the combustion chamber, and so is expected to decrease the amount of NO_x in the dual mode.

UHC pollutant is the sum of unburned hydrocarbons indicator and its existence is a sign of poor combustion. In diesel mode, the UHC content is reduced to the lowest level because of the presence of extra air inside the combustion chamber. In dual mode, and especially at part loads, the temperature of the combustion chamber is lower than that of the full loads, thus a high emission of UHC is expected under these conditions. Moreover, the in-cylinder wall temperature may be lower than the NG

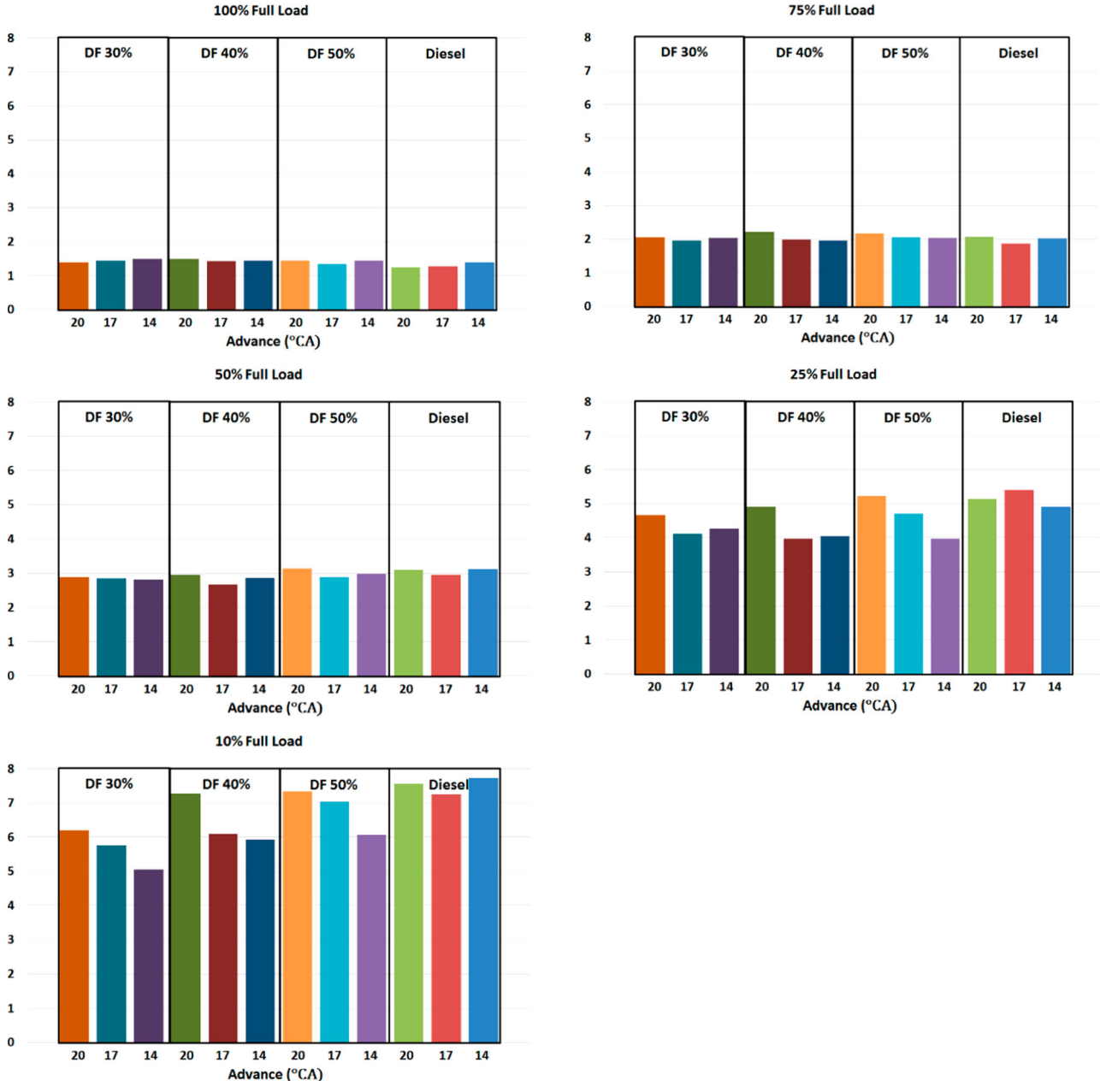

Figure 7. Lambda for different pilot injection timings and quantities.

ignition temperature, and thereby cause high emission of UHC.

In general, the best operation conditions are reached at part load while the most critical conditions are at low loads. The diesel engine does not have a throttle to restrict NG–air flow rate (or air only in diesel mode), and therefore at low load, the mixture becomes too lean, and so the ignition limits are not reached. This operating condition leads to high UHC emissions and low efficiency. At full load, there is at least one ignition start point for each diesel injector hole, meaning that the combustion speed can become too high so as to induce knocking, even with a high methane octane number of about 130 (Abagnale et al., 2014b). So, in the dual mode, especially at part loads, the UHC content rises significantly. Figure 6 shows the UHC emission under different loads, pilot injection timings and quantities.

According to Figure 6, the emission of UHC in dual mode is more than the diesel mode for all the test conditions, especially for part loads. Increasing the pilot injection timing gives enough time to mix the pilot fuel with the gaseous fuel and ignite it to achieve high performance combustion. For part loads increasing the pilot fuel increases the temperature of

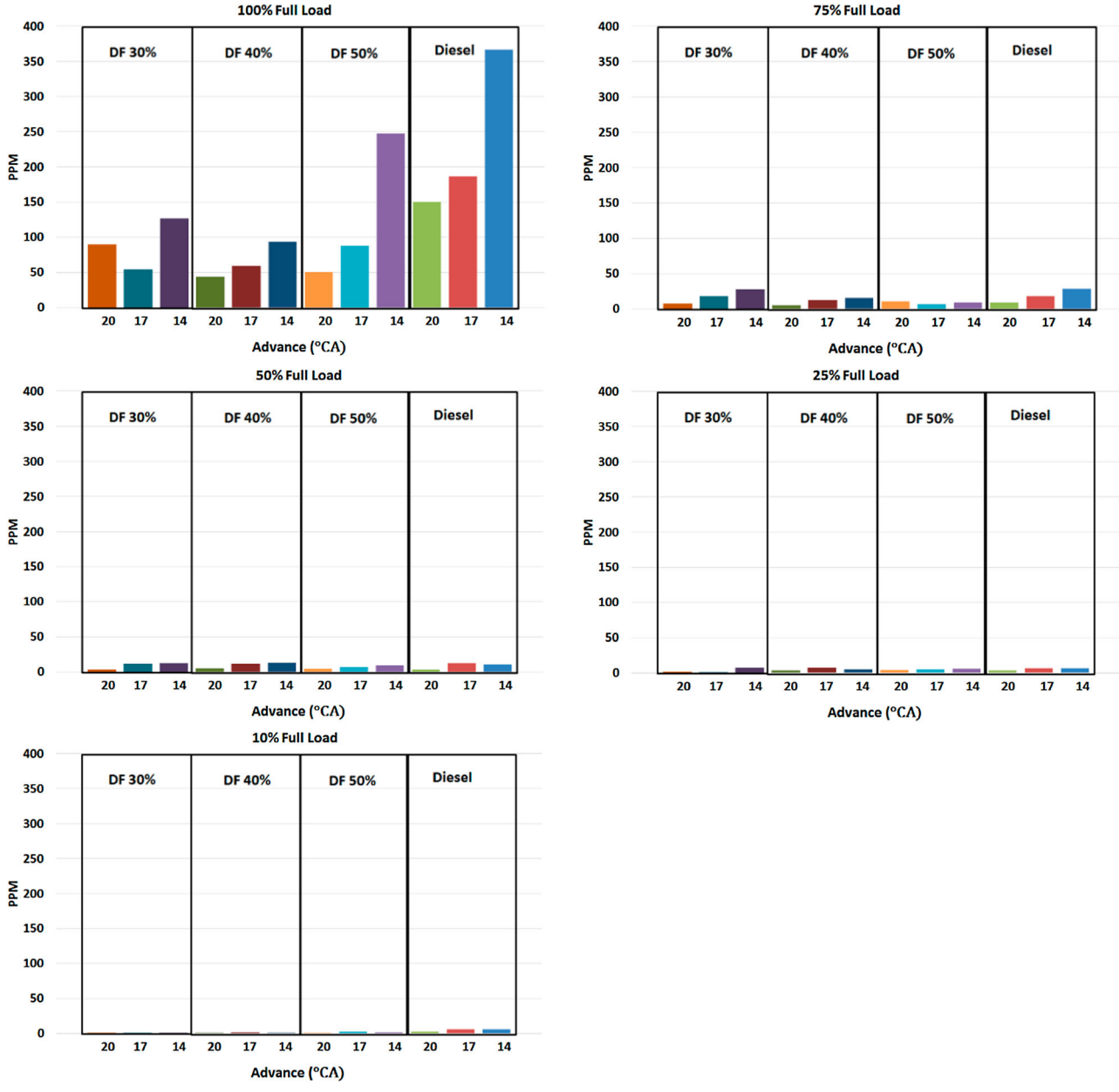

Figure 8. PM emission based on injection timings.

the combustion chamber, and the UHC content is expected to be reduced. In the dual mode, advancing the pilot injection timing decreases the UHC emission, but decreasing the pilot injection quantity increases it.

Variation of lambda (air–fuel ratio) calculated by Equation (9) (Ryu, 2013):

$$\lambda_{\text{total}} = \frac{\dot{m}_{\text{air}}}{(AFR_{\text{NG}})_{\text{Stoic}}.\dot{m}_{\text{NG}} + (AFR_{\text{PF}})_{\text{Stoic}}.\dot{m}_{\text{PF}}} \quad (9)$$

Figure 7 shows the results of the variation in lambda. For part loads and lower pilot injection quantities, the lambda increases. Increasing the pilot injection timing decreases the lambda especially under part loads, but diesel–gaseous fuel ratios have a negligible effect on lambda value at full load.

According to Figure 8 which shows the trend of the PM emission, the dual mode has lower PM emission than the diesel mode. As shown in Figure 8, at up to 80% of full load, the PM emission is similar in both diesel and dual modes under all test conditions because of the presence of enough air in the combustion chamber (lambda value in Figure 7) and good combustion. Under full load, the lambda value is about 1 and smoke limit in the diesel

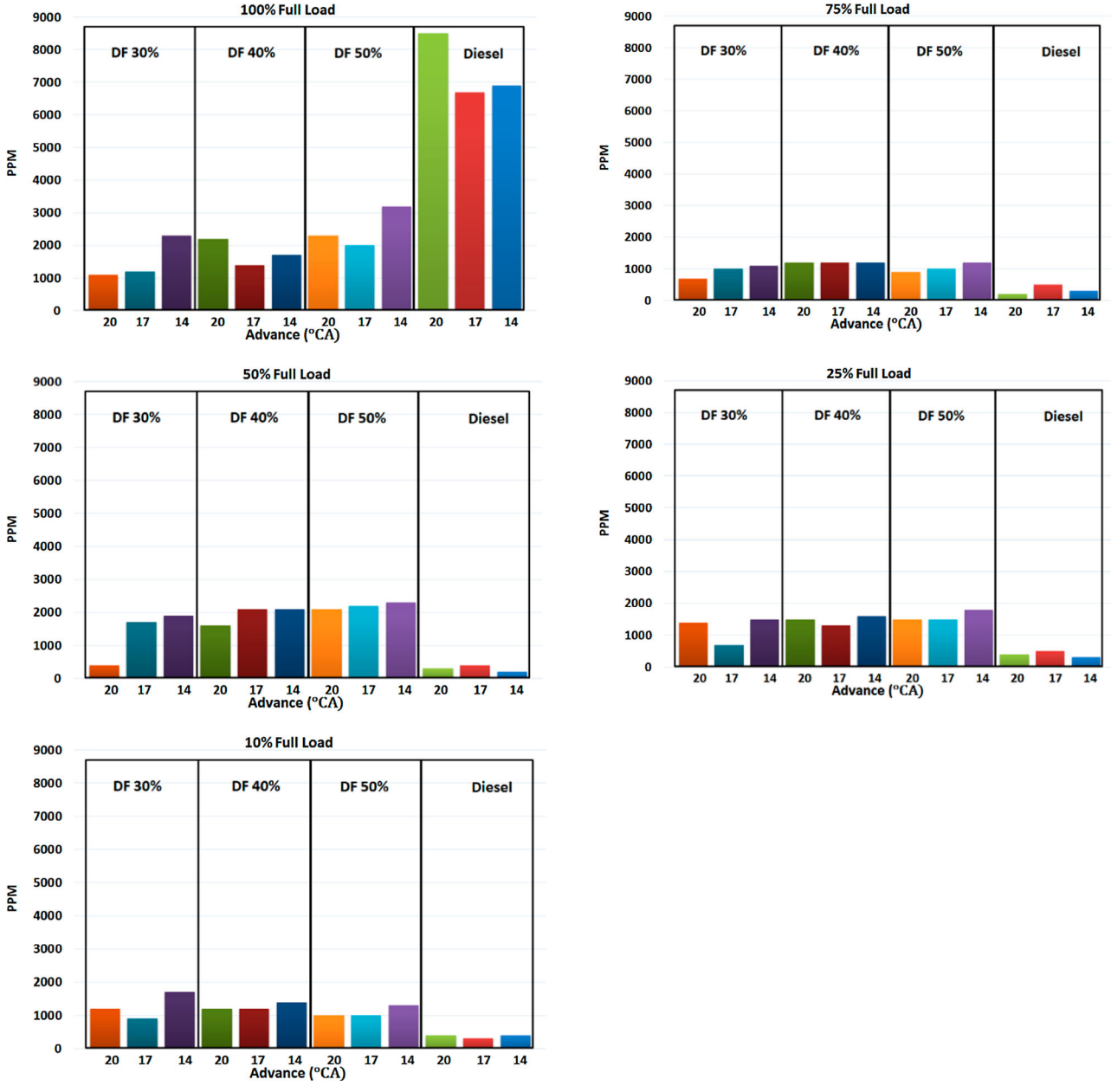

Figure 9. CO emission based on injection timings.

engine is about 1.4, so the PM emission rises in the diesel mode. In the dual mode, the pilot injection quantity decreases (up to 30%) and methane molecules replace the diesel fuel molecules and cause lower PM emission in comparison to the diesel mode. Increasing gaseous fuel and decreasing diesel fuel decreases the PM quantity, and increasing the pilot FIT decreases PM emission, especially under full load.

For up to 75% of the full load in the dual mode, CO emission is more than that for diesel mode, but at full load, the CO emission of diesel mode is more than that for the dual mode (Figure 9). Increasing the injection timing increases the CO emission in the diesel mode but decreases it in the dual mode. Up to 75% of the full load, the CO emission of dual mode is more than that for the diesel mode. At full load, the good combustion of gaseous (Figure 6) UHC pollutant increases the amount of CO emission. Under full load, decreasing the pilot injection quantity decreases CO emission, and increasing the pilot injection timing decreases CO emission under the most test conditions.

Brake specific energy consumption (BSEC) is calculated by Equation (10) (Hassan, Mohd Nor, Zainal, & Miskam, 2011):

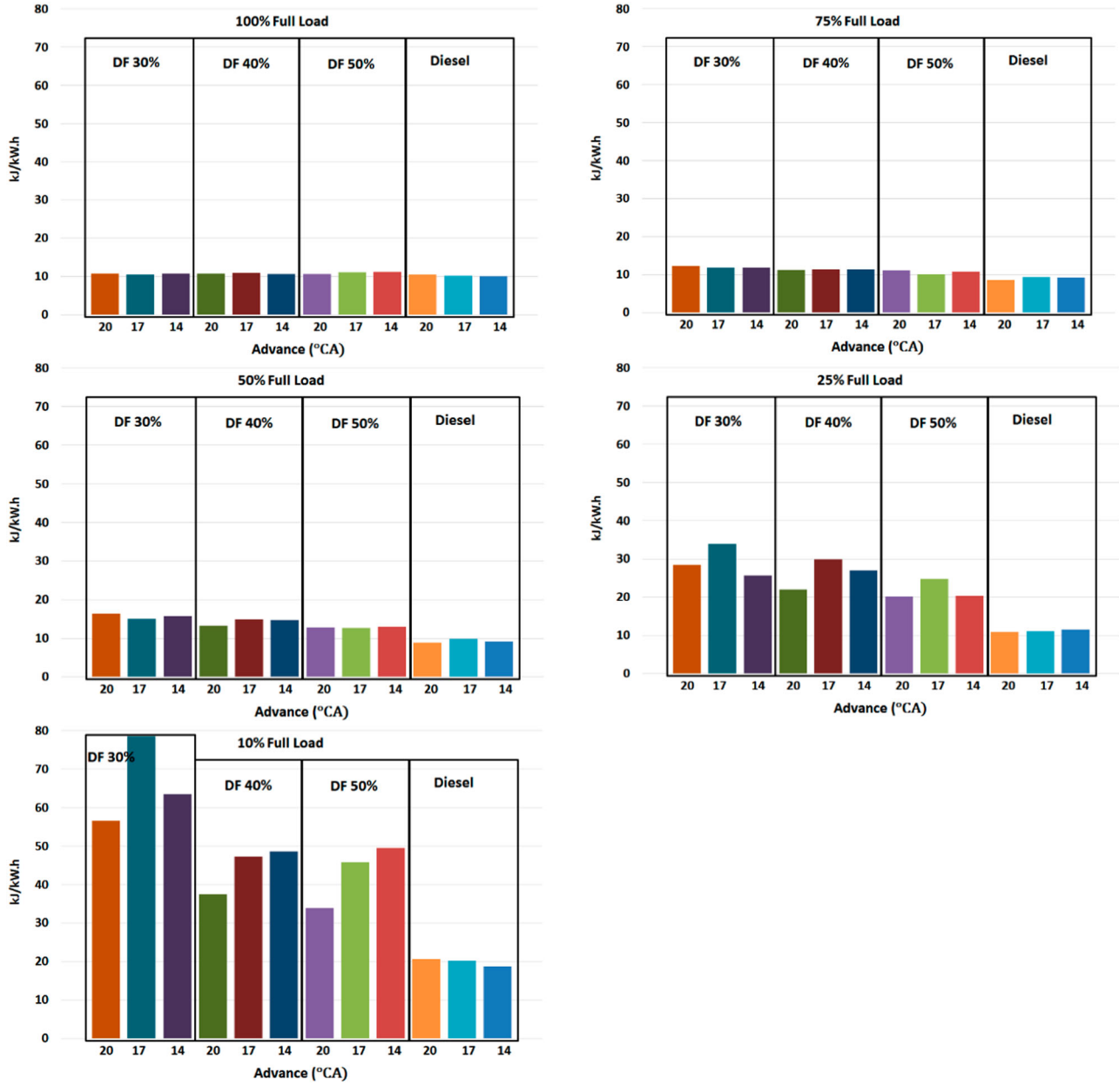

Figure 10. BSEC based on injection timings.

$$\text{BSEC} = \frac{\dot{H}_{\text{Pilotfuel}} + \dot{H}_{\text{NG}}}{\text{Power}} = \frac{\dot{m}_{\text{Pilotfuel}} \times \text{LHV}_{\text{Pilotfuel}} + \dot{m}_{\text{NG}} \times \text{LHV}_{\text{NG}}}{\text{Power}} \quad (10)$$

In the dual-fueled engine, BSEC is a good parameter to compare two different fuels. Results of BSEC are shown in Figure 10. The results show that the BSFC difference between the diesel and the dual modes is negligible and is close to each other for full loads. For part loads, however, BSEC of dual mode is higher than that for diesel mode. The reason can be related to UHC since the UHC emission for part loads increases and fuel energy is not completely released (Figure 6).

Figure 11 shows the in-cylinder pressures for different pilot injection timings and PGF ratios at full load. The $P-\theta$ diagrams are means of 50 cycles pressure in the cylinder. $P-\theta$ diagrams show that increasing the diesel FIT increases the in-cylinder pressure in both the diesel and the dual modes. The engine speed and loads were regulated to be constant for all of the test conditions. Therefore, increasing the injection timing of pilot fuel increases the in-cylinder pressure, and fuel consumption is expected to be reduced. Fuel consumption was reduced by increasing the pilot FIT as observed in the experimental tests. Decreasing the pilot injection advances the timing, increases combustion delay, and accordingly raises the cylinder pressure. The behavior of the $P-\theta$ diagrams in the dual mode was similar to that of the diesel mode in terms of pilot injection timing variations (14, 17, 20 degrees before TDC). In the dual mode, the combustion delay time was greater than that of the diesel mode. The $P-\theta$ diagrams in the dual mode, especially for part loads, show unusual combustion, which is caused by high levels of UHC, CO, and CO_2 emissions.

The extracted information of combustion chamber geometry from the ICEM software was imported to the KIVA 3V then the in-cylinder pressure and temperature and the HRR at various degrees of crankshaft were identified. Figure 12 shows the simulation results for

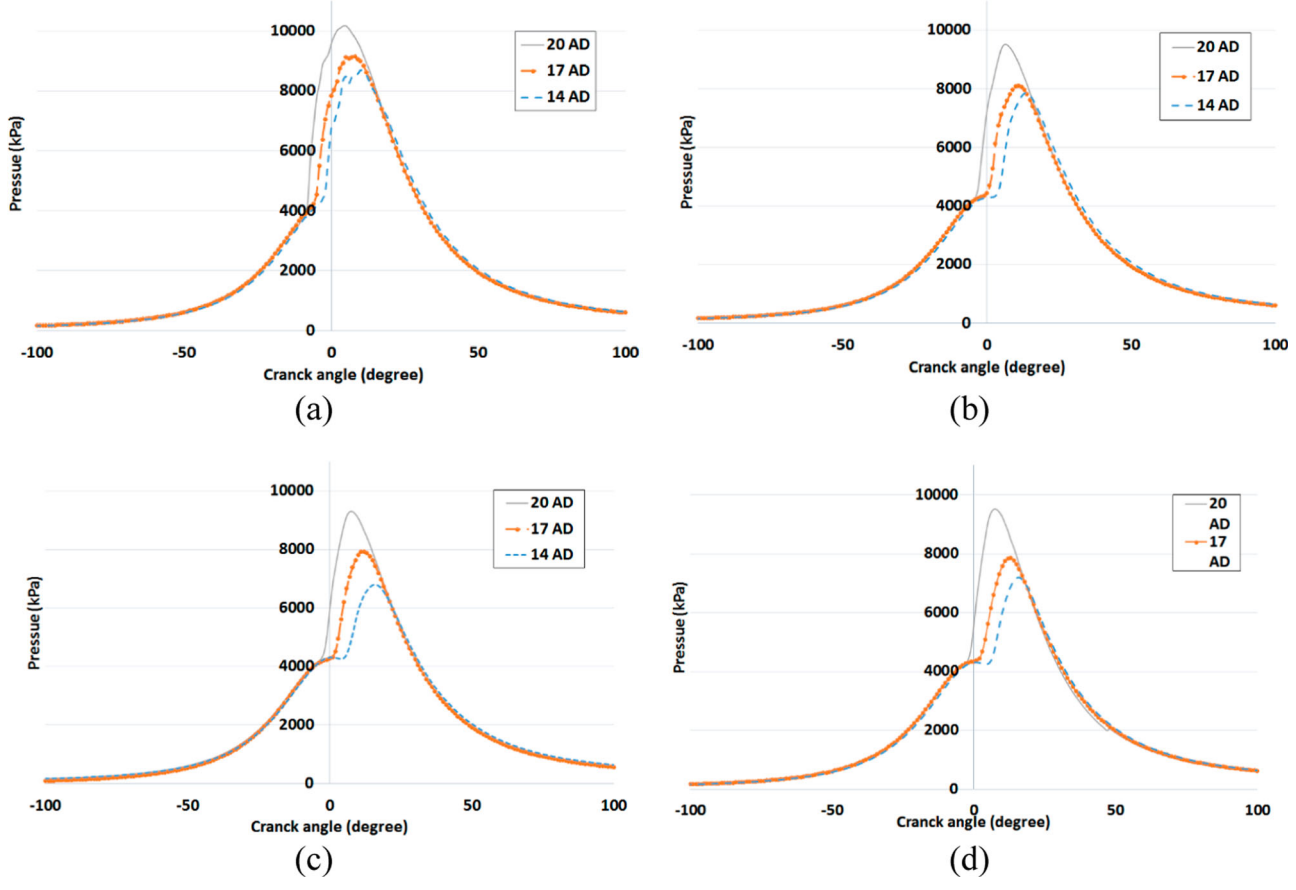

Figure 11. Cylinder pressure in full load and different advance timings, diesel mode (a), dual mode with 50% diesel (b), dual mode with 40% diesel (c), and dual mode with 30% diesel (d).

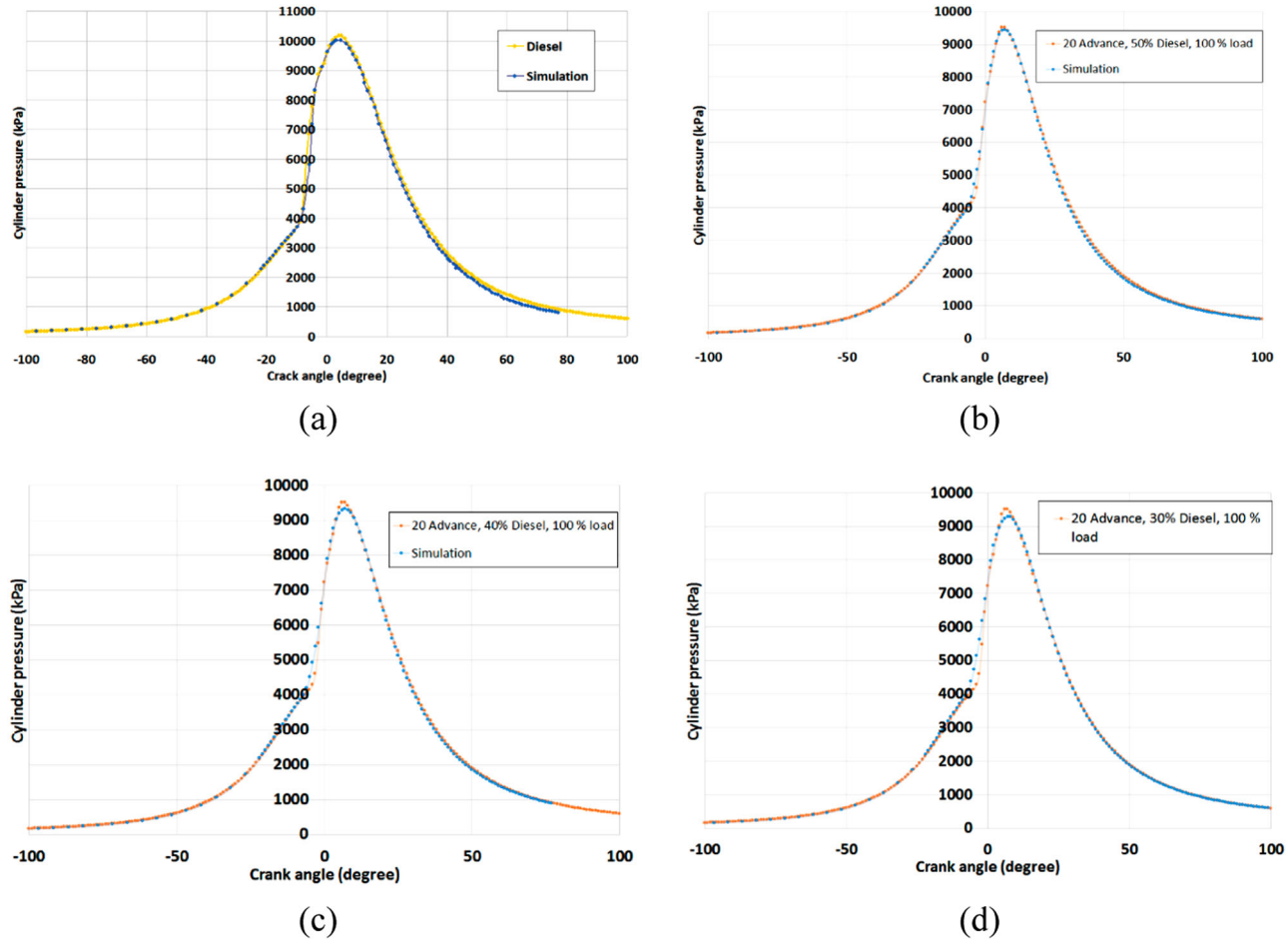

Figure 12. Experimental and simulation results of cylinder pressure in: (a) diesel mode, (b) dual mode with 50% diesel, (c) dual mode with 40% diesel, and (d) dual mode with 30% diesel.

in-cylinder pressure. The results of simulation had a good agreement with the experimental results.

HRR and cylinder temperature were simulated with KIVA-3V code and the results are shown in Figure 13. The increase in the cylinder temperature in the diesel mode was faster than in the dual mode, although the cumulative cylinder temperature in the diesel mode was lower than that for the dual mode. This means that the diesel fuel combustion rate is higher than that of gaseous fuel (methane), and thus while using the dual fuel mode, there is a need to increase the pilot fuel advance timing to increase the cylinder pressure in TDC. Since the ID in the dual mode is more than that of the diesel mode, the HRR in the diesel mode is faster than that of the dual mode. As shown in Figure 13, the increasing temperature rate in the diesel mode is higher than that of the dual mode so it is expected that the NO_x emission in diesel engine will be more than that of the dual mode, as confirmed by the experimental results for NO_x emission (Figure 5).

The simulation results at TDC are shown in Figures 14 and 15. Due to the lower ID time in the diesel mode as compared to the dual mode, the cylinder pressure and temperature in the diesel mode at TDC is higher than those for the dual mode.

As shown in Figure 15, combustion in the diesel mode starts earlier than in the dual mode and continues thereafter. These phenomena can be explained by the natural gas characteristic of a higher auto-ignition temperature compared to diesel fuel.

Conclusions

In this study, a constant speed diesel engine was modified to function as a dual-fueled diesel engine. NG was used as the base fuel and diesel fuel was considered as the pilot fuel. The experimental tests were carried out for performance and emissions under different loads (10, 25, 50, 75, and 100% of the full load) and PGF ratios (30, 40 and 50%). Based on the results, at a constant

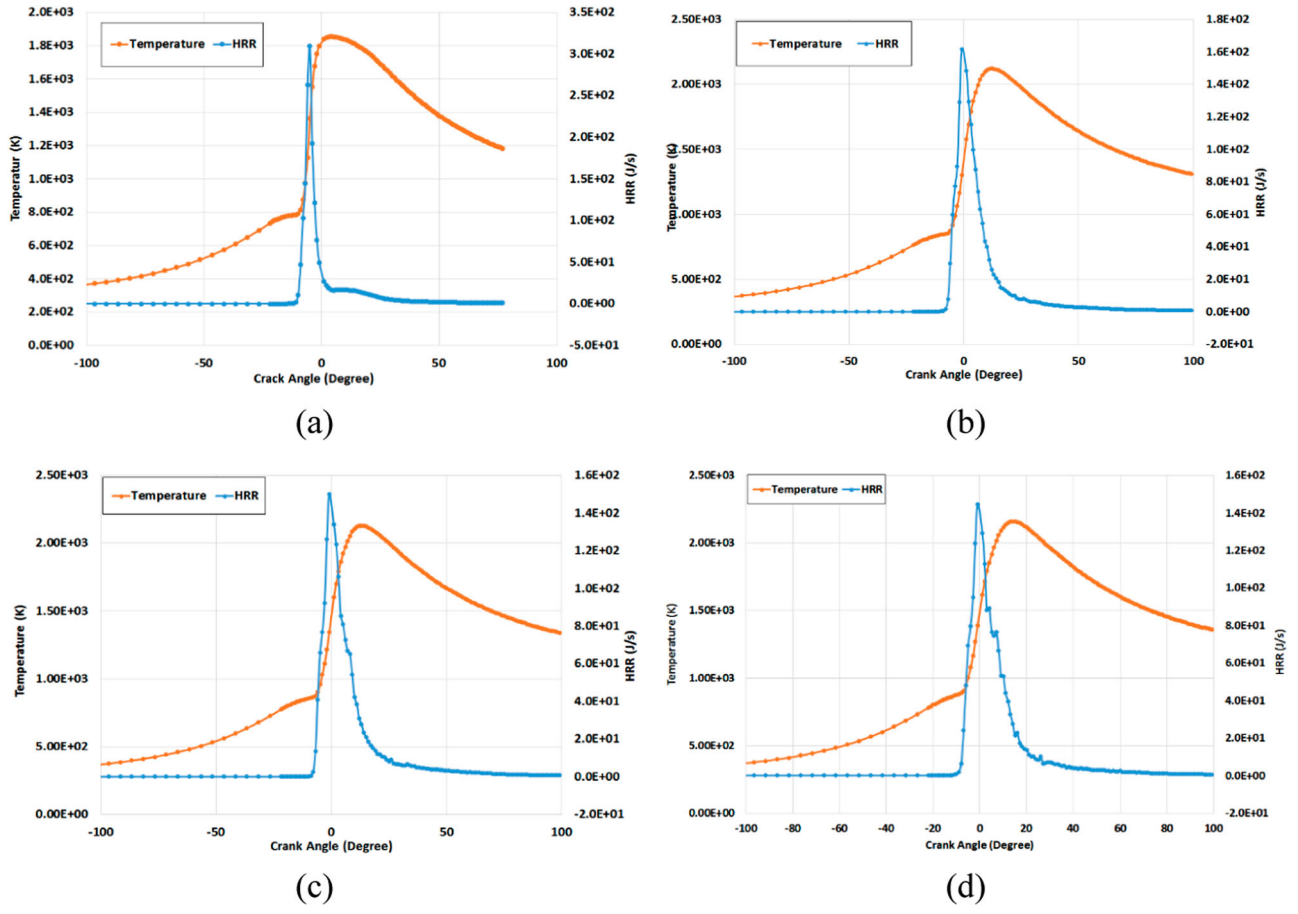

Figure 13. Simulation results for HRR and cumulative temperature in: (a) diesel mode, (b) dual mode with 50% diesel, (c) dual mode with 40% diesel, and (d) dual mode with 30% diesel.

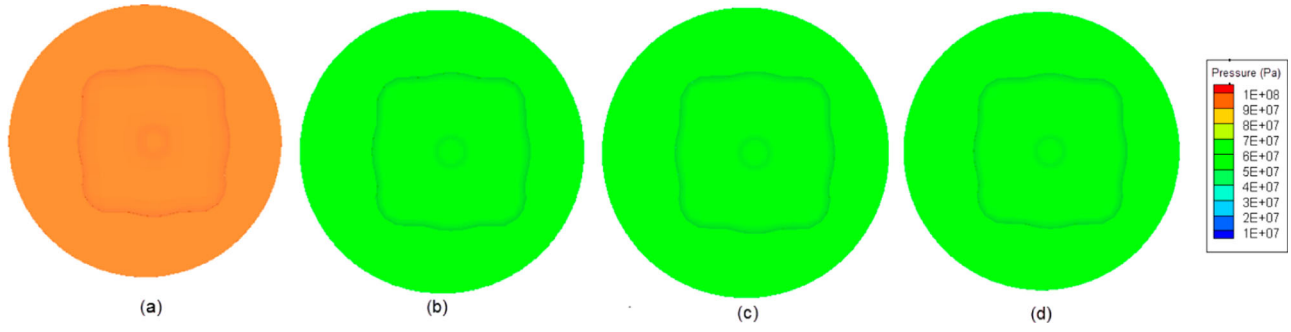

Figure 14. Simulation results for cylinder pressure at TDC for 20 degree advance timing in: (a) diesel mode, (b) dual mode with 50% diesel, (c) dual mode with 40% diesel, and (d) dual mode with 30% diesel.

speed of the engine with variable loads, the dual-fueled mode had lower CO_2, NO_x, and PM emissions under all load conditions and PGF ratios when compared to diesel mode. At full load, the dual-fueled engine had relatively lower CO emission and higher HC emission. Also, under full load, the specific energy consumption of the dual-fueled engine was similar to that for the diesel engine.

For reducing emissions as well as better fuel economy, it is suggested to use an engine in the dual mode at 30 and 50% of the pilot fuel ratio in full and half loads, respectively.

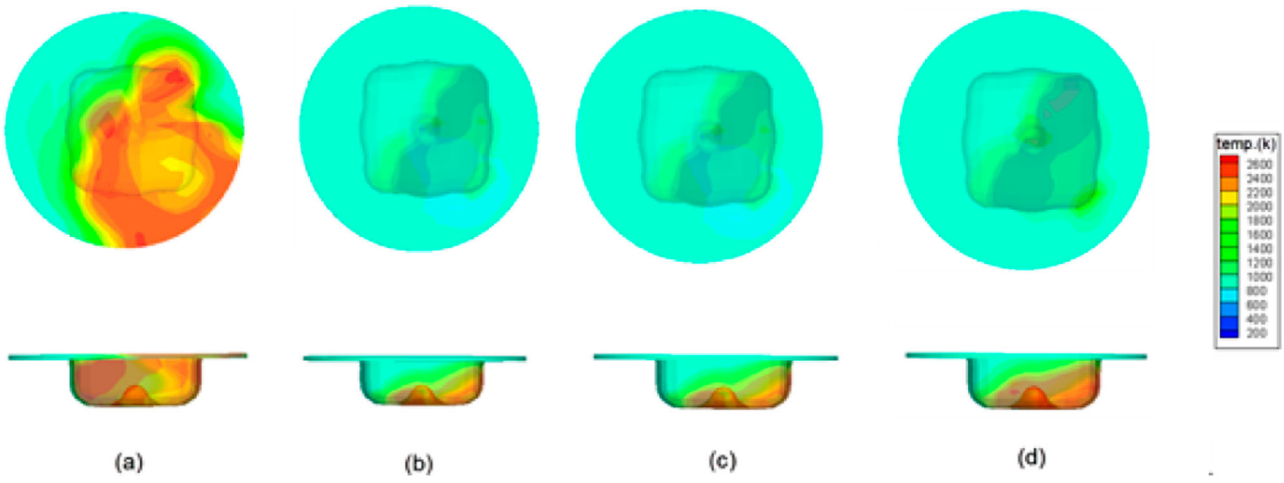

Figure 15. Simulation results for cylinder temperature at TDC for 20 degree advance timing in: (a) diesel mode, (b) dual mode with 50% diesel, (c) dual mode with 40% diesel, and (d) dual mode with 30% diesel.

Modifying the KIVA code could enable the estimation of simulations of cylinder pressure and emissions perfectly in the dual mode, and they demonstrated a good agreement with the experimental results.

Disclosure statement

No potential conflict of interest was reported by the authors.

ORCID

Sina Faizollahzadeh Ardabili http://orcid.org/0000-0002-7744-7906
Shahaboddin Shamshirband http://orcid.org/0000-0002-6605-498X

References

Abagnale, C., Cameretti, M. C., De Simio, L., Gambino, M., Iannaccone, S., & Tuccillo, R. (2014a). Combined numerical-experimental study of dual fuel diesel engine. *Energy Procedia*, *45*, 721–730. doi:10.1016/j.egypro.2014.01.077

Abagnale, C., Cameretti, M. C., De Simio, L., Gambino, M., Iannaccone, S., & Tuccillo, R. (2014b). Numerical simulation and experimental test of dual fuel operated diesel engines. *Applied Thermal Engineering*, *65*(1–2), 403–417. doi:10.1016/j.applthermaleng.2014.01.040

Arteconi, A., Brandoni, C., Evangelista, D., & Polonara, F. (2010). Life-cycle greenhouse gas analysis of LNG as a heavy vehicle fuel in Europe. *Applied Energy*, *87*(6), 2005–2013.

Barik, D., & Murugan, S. (2014). Simultaneous reduction of NOx and smoke in a dual fuel DI diesel engine. *Energy Conversion and Management*, *84*, 217–226. doi:10.1016/j.enconman.2014.04.042

Di Iorio, S., Magno, A., Mancaruso, E., & Vaglieco, B. M. (2016). Characterization of particle number and mass size distributions from a small compression ignition engine operating in diesel/methane dual fuel mode. *Fuel*, *180*, 613–623. doi:10.1016/j.fuel.2016.04.108

Di Iorio, S., Magno, A., Mancaruso, E., & Vaglieco, B. M. (2017). Analysis of the effects of diesel/methane dual fuel combustion on nitrogen oxides and particle formation through optical investigation in a real engine. *Fuel Processing Technology*, *159*, 200–210.

Ge, J. C., Kim, M. S., Yoon, S. K., & Choi, N. J. (2015). Effects of pilot injection timing and EGR on combustion, performance and exhaust emissions in a common rail diesel engine fueled with a canola oil biodiesel-diesel blend. *Energies*, *8*, 7312–7325. doi:10.3390/en8077312

Hassan, S., Mohd Nor, F., Zainal, Z. A., & Miskam, M. A. (2011). Performance and emission characteristics of supercharged biomass producer gas-diesel dual fuel engine. *Journal of Applied Sciences*, *11*, 1606–1611.

Jamuwa, D. K., Sharma, D., & Soni, S. L. (2016). Experimental investigation of performance, exhaust emission and combustion parameters of stationary compression ignition engine using ethanol fumigation in dual fuel mode. *Energy Conversion and Management*, *115*, 221–231. doi:10.1016/j.enconman.2016.02.055

Jung, J., Song, S., & Hur, K. B. (2017). Numerical study on the effects of intake valve timing on performance of a natural gas-diesel dual-fuel engine and multi-objective pareto optimization. *Applied Thermal Engineering*, *96*, 121–134.

Kumar, K. S., & Raj, R. T. K. (2013). Effect of fuel injection timing and elevated intake air temperature on the combustion and emission characteristics of dual fuel operated diesel engine. *Procedia Engineering*, *64*, 1191–1198. doi:10.1016/j.proeng.2013.09.198

Lata, D. B., & Misra, A. (2010). Theoretical and experimental investigations on the performance of dual fuel diesel engine with hydrogen and LPG as secondary fuels. *International Journal of Hydrogen Energy*, *35*(21), 11918–11931. doi:10.1016/j.ijhydene.2010.08.039

Lee, S., & Park, S. (2017). Optimization of the piston bowl geometry and the operating conditions of a gasoline-diesel dual-fuel engine based on a compression ignition engine. *Energy*, *121*, 433–448.

Ling, S., Longbao, Z., Shenghua, L., & Hui, Z. (2005). Decreasing hydrocarbon and carbon monoxide emissions of a natural-gas engine operating in the quasi-homogeneous

charge compression ignition mode at low loads. *Proceedings of the Institution of Mechanical Engineers, Part D: Journal of Automobile Engineering*, *219*, 1125–1131.

Lipardi, A. C. A., Versailles, P., Watson, G. M. G., Bourque, G., & Bergthorson, J. M. (2017). Experimental and numerical study on NOx formation in CH4–air mixtures diluted with exhaust gas components. *Combustion and Flame*, *179*, 325–337. doi:10.1016/j.combustflame.2017.02.009

Lounici, M. S., Boussadi, A., Loubar, K., & Tazerout, M. (2014). Experimental investigation on NG dual fuel engine improvement by hydrogen enrichment. *International Journal of Hydrogen Energy*, *39*(36), 21297–21306. doi:10.1016/j.ijhydene.2014.10.068

Lounici, M. S., Loubar, K., Tarabet, L., Balistrou, M., Niculescu, D.-C., & Tazerout, M. (2014). Towards improvement of natural gas-diesel dual fuel mode: An experimental investigation on performance and exhaust emissions. *Energy*, *64*, 200–211. doi:10.1016/j.energy.2013.10.091

Maghbouli, A., Saray, R. K., Shafee, S., & Ghafouri, J. (2013). Numerical study of combustion and emission characteristics of dual-fuel engines using 3D-CFD models coupled with chemical kinetics. *Fuel*, *106*, 98–105. doi:10.1016/j.fuel.2012.10.055

Mikulski, M., & Wierzbicki, S. (2016). Numerical investigation of the impact of gas composition on the combustion process in a dual-fuel compression-ignition engine. *Journal of Natural Gas Science and Engineering*, *31*, 525–537. doi:10.1016/j.jngse.2016.03.074

Mintz, M., Han, J., & Burnham, A. (2014). Alternative and renewable gaseous fuels to improve vehicle environmental performance. In R. Folkson (Ed.), *Alternative fuels and advanced vehicle technologies for improved environmental performance* (pp. 90–116). New York: Woodhead Publishing.

Mittal, M., Donahue, R., Winnie, P., & Gillette, A. (2015). Exhaust emissions characteristics of a multi-cylinder 18.1-L diesel engine converted to fueled with natural gas and diesel pilot. *Journal of the Energy Institute*, *88*(3), 275–283. doi:10.1016/j.joei.2014.09.003

Murty, K. A. (1975). *Introduction to combustion phenomena* (Vol. 2). Boca Raton, FL: CRC Press.

Mustafi, N. N., Raine, R. R., & Verhelst, S. (2013). Combustion and emissions characteristics of a dual fuel engine operated on alternative gaseous fuels. *Fuel*, *109*, 669–678. doi:10.1016/j.fuel.2013.03.007

Najafi, B. (2011). Experimental investigation of the effect of using biodiesel and biogas on dual fuel diesel engine.

Najafi, B., Piirouzpanah, V., Ghobadian, B., Sadegpour, & Ranjbar, A. (2007). Experimental investigation of diesel engine performance parameters and pollution using biodiesel.

Najafi, B., Torkian, M., Hejazi, M., & Zamzamian, A. (2011). Effect of microalgae biodiesel on performance parameters and exhaust emissions from IDI diesel engine.

Pan, W., Yao, C., Han, G., Wei, H., & Wang, Q. (2015). The impact of intake air temperature on performance and exhaust emissions of a diesel methanol dual fuel engine. *Fuel*, *162*, 101–110. doi:10.1016/j.fuel.2015.08.073

Papagiannakis, R. G. (2013). Study of air inlet preheating and EGR impacts for improving the operation of compression ignition engine running under dual fuel mode. *Energy Conversion and Management*, *68*, 40–53. doi:10.1016/j.enconman.2012.12.019

Papagiannakis, R. G., & Hountalas, D. T. (2003). Experimental investigation concerning the effect of natural gas percentage on performance and emissions of a DI dual fuel diesel engine. *Applied Thermal Engineering*, *23*(3), 353–365. doi:10.1016/S1359-4311(02)00187-4

Papagiannakis, R. G., & Hountalas, D. T. (2004). Combustion and exhaust emission characteristics of a dual fuel compression ignition engine operated with pilot diesel fuel and natural gas. *Energy Conversion and Management*, *45*(18–19), 2971–2987. doi:10.1016/j.enconman.2004.01.013

Pedrozo, V. B., May, I., Dalla Nora, M., Cairns, A., & Zhao, H. (2016). Experimental analysis of ethanol dual-fuel combustion in a heavy-duty diesel engine: An optimisation at low load. *Applied Energy*, *165*, 166–182. doi:10.1016/j.apenergy.2015.12.052

Prakash, G., Shaik, A. B., & Ramesh, A. (1999). An approach for estimation of ignition delay in a dual fuel engine. *In: SAE technical paper 990232*, *1*, 1–7.

Rosen, A. (1989). *KIVA-II: A computer program for chemically reactive flows with sprays*. New Mexico: Los Alamos National Laboratory: University of California for the United States.

Ryu, K. (2013). Effects of pilot injection timing on the combustion and emissions characteristics in a diesel engine using biodiesel–CNG dual fuel. *Applied Energy*, *111*, 721–730. doi:10.1016/j.apenergy.2013.05.046

Sahoo, B. B., Sahoo, N., & Saha, U. K. (2009). Effect of engine parameters and type of gaseous fuel on the performance of dual-fuel gas diesel engines—A critical review. *Renewable and Sustainable Energy Reviews*, *13*(6–7), 1151–1184. doi:10.1016/j.rser.2008.08.003

Singh Kalsi, S., & Subramanian, K. A. (2016). Experimental investigations of effects of EGR on performance and emissions characteristics of CNG fueled reactivity controlled compression ignition (RCCI) engine. *Energy Conversion and Management*, *130*, 91–105.

Tarabet, L., Loubar, K., Lounici, M. S., Khiari, K., Belmrabet, T., & Tazerout, M. (2014). Experimental investigation of DI diesel engine operating with eucalyptus biodiesel/natural gas under dual fuel mode. *Fuel*, *133*, 129–138. doi:10.1016/j.fuel.2014.05.008

Turns, S. R. (2000). An introduction to combustion concepts and applications.

Wang, Z., Chen, W., Wang, D., Tan, M., Liu, Z., & Dou, H. (2016). A novel combustion evaluation method based on in-cylinder pressure traces for diesel/natural gas dual fuel engines. *Energy*, *115*, 1130–1137.

Yaliwal, V. S., Banapurmath, N. R., Gireesh, N. M., Hosmath, R. S., Donateo, T., & Tewari, P. G. (2016). Effect of nozzle and combustion chamber geometry on the performance of a diesel engine operated on dual fuel mode using renewable fuels. *Renewable Energy*, *93*, 483–501. doi:10.1016/j.renene.2016.03.020

Yang, B., Xi, C., Wei, X., Zeng, K., & Lai, M.-C. (2015). Parametric investigation of natural gas port injection and diesel pilot injection on the combustion and emissions of a turbocharged common rail dual-fuel engine at low load. *Applied Energy*, *143*, 130–137. doi:10.1016/j.apenergy.2015.01.037

Yoon, S. K., Kim, M. S., Kim, H. J., & Choi, N. J. (2014). Effects of canola oil biodiesel fuel blends on combustion, performance, and emissions reduction in a common rail diesel engine. *Energies*, *7*, 8132–8149. doi:10.3390/en7128132

Yoon, S. H., & Lee, C. S. (2011). Experimental investigation on the combustion and exhaust emission characteristics of biogas–biodiesel dual-fuel combustion in a CI engine. *Fuel Processing Technology*, *92*(5), 992–1000. doi:10.1016/j.fuproc.2010.12.021

Zhang, C.-h., & Song, J.-t. (2016). Experimental study of co-combustion ratio on fuel consumption and emissions of NG–diesel dual-fuel heavy-duty engine equipped with a common rail injection system. *Journal of the Energy Institute*, *89*(4), 578–585. doi:10.1016/j.joei.2015.06.005

Zhao, Y., Wang, Y., Li, D., Lei, X., & Liu, S. (2014). Combustion and emission characteristics of a DME (dimethyl ether)-diesel dual fuel premixed charge compression ignition engine with EGR (exhaust gas recirculation). *Energy*, *72*, 608–617. doi:10.1016/j.energy.2014.05.086